RESEARCH ARTICLE | AUGUST 18 2022

Nonevaporable getter-MEMS for generating UHV conditions in small volumina

Special Collection: Vacuum Nanoelectronics

Leonard Frank Diekmann; Alexander Kassner; Folke Dencker; ... et. al

Check for updates

Journal of Vacuum Science & Technology B 40, 054202 (2022)
https://doi.org/10.1116/6.0001991

CrossMark

View Online

Export Citation

Related Content

Activation volume for self-diffusion and for the diffusion of impurities in lead

Journal of Applied Physics (July 2008)

Low-cost, high-performance nonevaporable getter pumps using nonevaporable getter pills

Journal of Vacuum Science & Technology A (August 2016)

Evaluation of Zr–V–Fe getter pump for UHV system

Journal of Vacuum Science & Technology A (April 1983)

Downloaded from http://pubs.aip.org/avs/jvb/article-pdf/doi/10.1116/6.0001991/16612541/054202_1_online.pdf

JVST B
Journal of Vacuum Science & Technology B

ARTICLE

avs.scitation.org/journal/jvb

Nonevaporable getter-MEMS for generating UHV conditions in small volumina

Cite as: J. Vac. Sci. Technol. B **40**, 054202 (2022); doi: 10.1116/6.0001991
Submitted: 25 May 2022 · Accepted: 13 July 2022 ·
Published Online: 18 August 2022

Leonard Frank Diekmann,[a] Alexander Kassner, Folke Dencker, and Marc Christopher Wurz

AFFILIATIONS

Institut of Micro Production Technology, Leibniz University of Hannover, An der Universität 2, 30823 Garbsen, Lower Saxony, Germany

Note: This paper is a part of the 2023 Special Topic Collection on Vacuum Nanoelectronics.
[a]**Author to whom correspondence should be addressed:** Diekmann@impt.uni-hannover.de

ABSTRACT

The industrial use of quantum sensors requires further miniaturization of the experimental peripherals, i.e., the high vacuum chamber, laser technology, and control electronics. A central part of the high vacuum chamber is the maintenance of vacuum conditions. For this purpose, a prototype of a compact, i.e., miniaturized, ultrahigh vacuum pump in the form of a nonevaporable getter (NEG) pump at a wafer level (MEMS), is developed within the scope of this work. With regard to the basic conditions of the functionality of the NEG, a miniaturized heating plate with temperature sensors is analytically and numerically developed, constructed, and characterized in an ultrahigh vacuum test stand. This is followed by the integration of the NEG into the existing system, which, in connection with the characterization of material-specific parameters, enables a first correlation of heat input and pumping power. Thus, performance data of the getter-MEMS under high-vacuum confinement confirm its usability for quantum sensors. In addition, optimization potentials are shown with regard to all partial aspects of the MEMS.

© 2022 Author(s). All article content, except where otherwise noted, is licensed under a Creative Commons Attribution (CC BY) license (http://creativecommons.org/licenses/by/4.0/). https://doi.org/10.1116/6.0001991

Downloaded from http://pubs.aip.org/avs/jvb/article-pdf/doi/10.1116/6.0001991/16612541/054202_1_online.pdf

I. INTRODUCTION

Magneto-optical traps (MOTs) enable the cooling and trapping of atoms with the help of laser cooling and Zeeman splitting in a magnetic field and, thus, the generation of ultracold matter. In doing so, these neutral particles can change into the aggregate state of the Bose–Einstein condensate, from which special quantum mechanical properties result. These form the basis for a wide variety of technological applications, e.g., atomic wave interferometry. Since the formulation of quantum physics, experimental methods and theoretical understanding of laboratory quantum physics have advanced to such an extent that ultracold matter is ready to find industrial applications in the form of new, miniaturized quantum sensors. The quantum system generally consists of a so-called atomchip, a high vacuum chamber, a laser system, and suitable control electronics. At the current stage of miniaturization, the development of a miniaturized MOT is aimed for and advancing, which, in particular, requires complete miniaturization of a suitable high vacuum chamber and the integration of all other components in it.[1]

For the technical functionality of the quantum sensor, a vacuum level of 10^{-7}–10^{-13} mbar must be generated and maintained.[2] Sealing the system under these vacuum conditions guarantees a basic pressure level.[1] In order to maintain recipient pressure and associated functions, natural and artificial sources of leakage must be minimized and compensated. Natural sources of leakage include the permeability along (non) cohesive connections of the chamber components, especially the connection joints and optical components. Artificial leakage sources include the outgassing of chamber components. Here, MEMS adsorption pumps based on a nonevaporable getter (NEG) represent a major component for the high vacuum technology. In contrast to the vaporizable getters (flash getters), the NEGs neither induce increased vibrations nor degrade the optical components (e.g., gratings) in the recipient through particle deposits. These NEGs not only enable the evacuation of the main gaseous components of the vacuum atmosphere, but also minimize the outgassing of the surfaces coated with them by interacting chemically and physically with molecules in the atmosphere.[3] In general, NEG coatings have proven to be useful for extreme

and ultrahigh vacuum applications by already being part of modern vacuum systems, such as in the Large Hadron Collider (CERN).[4] As part of the experiment on ultracold matter, any magnetic interference fields must be minimized, which is why no magnetic materials are used as NEGs. Often, oxygen-affine or reactive metals or combinations of these are used instead. Due to the excellent intrinsic performance parameters (pumping power and bulk capacity), ternary and quaternary material combinations of TiZrV or TiZrHfV are used.[1,5]

The superficial atoms of the getter initially physically bind the components of the atmosphere, which is usually followed by forming a chemical, covalent and thus stable bond.[3] In order to initialize the NEG pumping function, cyclic supply of thermal energy (at least 160 °C for 12 h) is required after the surface has been saturated. This enables the molecules to diffuse along a concentration gradient into the bulk material.[4,6] One promising possibility is the supply of energy by means of Joule heating of a platinum resistor, which is calibrated following directive DIN 43764.[7] This technology has the advantage that the temperature can be introduced quickly, homogeneously, and precisely and at the same time can be monitored over a wide temperature range using four-wire technology. To ensure uniform heating functionality, a temperature sensor array is integrated into the heating system.

II. EXPERIMENT

A. Joule heating

The provision of the required energy for the activation of the getter is achieved in the form of heat, specifically in the form of a microheater element, also called a thermistor, using Joule heating. Joule heating is a physical effect in which an electrical current (I) generates thermal energy through an electrical conductor (also known as power dissipation P), which results in an increase in material temperature [T, Eq. (1)]. Knowing the material-specific heat capacity (c) and mass (m), the temperature change can be estimated with the help of the power introduced over time (t) [Eq. (2)],

$$P = R \times I^2, \tag{1}$$

$$\Delta T = P \times t\,(m \times c)^{-1}. \tag{2}$$

B. Pumping

NEGs (pumps) are classified as adsorption pumps and, therefore, have activation energy, pumping power S [Eq. (3)], storage capacity, and final pressure as performance parameters.

The activation energy of the NEG describes the supply of threshold energy in the form of heat (i.e., threshold temperature), which allows diffusion of the surface-bound, reactive atoms (oxygen, nitrogen, carbon) and their compounds into and through the material. This is complete as soon as the concentration of the reactive elements in the material has homogenized. In simplified terms, the progress of diffusion is element-specific and is defined by the absorbed energy dose, which is determined from the product of temperature and time.[8]

The pumping power S [Eq. (3)] generally describes the volumetric quantity that passes a defined area per unit of time. For adsorption pumps, such as the NEG, the pumping power describes how many particles can be absorbed and bound per unit of time at a specific temperature and pressure. The integral of the pumping power over time results in the capacity, i.e., the number of molecules that can be stored in the material. With ideal processing, this capacity depends on the crystal structure and proportionally on the layer height. The actual pumping process consists of two-stages. First, the reactive gas molecules are physically and (apart from hydrogen) then chemically bound to the surface of the NEG. Here, the total number of free bonds on the surface and the respective reactive behavior of the NEG elements defined the bonding probability of the reactive elements from the surrounding atmosphere. This number of free bonds on the surface per area describes the surface capacity, i.e., the quantitative ability to absorb the reactive residual gas components. This surface capacitance is defined by the surface morphology, which can be further defined using the standard roughness parameters, the arithmetic mean roughness value R_a, and the roughness depth R_z. Every regular pumping process changes the concentration of the reactive elements in the material. First, this means that the number of free bonds on the surface is reduced with each pumping process so that fewer reactive elements can be bound. Second, the increase in concentration caused by the pumping process leads to lengthening of the diffusion paths. The decisive factor here is the lengthening of the diffusion path, which is proportionally accompanied by an increase in the activation dose so that heating (activation) must either be longer or stronger to achieve the maximum pumping effect. Taking into account the total change in chamber pressure, the pumping power further derives (standardized) to the suction power Q [Eq. (4)]. The suction power of a pump describes the change in pressure of a defined volume of gas flowing (sucked off) through a defined area per time. An effective suction power can be calculated by adding the flow conductance of the vacuum environment.[8]

During the pumping process, under defined boundary conditions without a gas inlet, the pressure approaches the so-called final pressure asymptotically, which is usually lower than the base pressure achievable according to directive DIN ISO 21360,[9,10]

$$S = -\Delta V \times \Delta t^{-1}, \tag{3}$$

$$Q = S \times \Delta p. \tag{4}$$

C. UHV compatible test-chamber

For the characterization of the getter pump in a high vacuum, the setup and the characterization (vacuum properties) of its corresponding high vacuum level recipient and its components must first be carried out in order to guarantee a reproducible operating point for the investigation of the system. The structure is a small volume recipient (2 l) with a pump system, consisting of a membrane pump and a turbomolecular pump (HiPace 300H), a cold cathode pressure gauge (IKR 271),[10] a quadrupole mass spectrometer (HAL301 RGA, 301F 300 amu),[11] and the getter-MEMS slot, which consists of a CF-100 flange with electrical feedthroughs and a high vacuum wafer holder (Fig. 1).

The IKR 270 cold cathode pressure gauge is a gas-type-dependent measuring system that is calibrated for

Downloaded from http://pubs.aip.org/avs/jvb/article-pdf/doi/10.1116/6.0001991/16612541/054202_1_online.pdf

© Author(s) 2022

nitrogen using a reference standard according to DIN EN ISO 3567,[13] in this case a gas-type-independent, capacitive transmitter (Baratron). For other residual gas compositions (i.e., H_2 in UHV environments), there is the possibility of using a calibration factor according to the manufacturer. Overall, the gauge has an accuracy of ±30% in the pressure range of 10^{-3}–10^{-9} mbar.[10]

With the quadrupole mass spectrometer, gas molecules are ionized by thermally generated electrons, which are then differentiated by a mass filter and detected in a Faraday cage or a secondary electron multiplier detector thereafter. The system is calibrated for nitrogen to an ion current of 10^{-4} A mbar^{-1} so that at a pressure of 10^{-11} mbar, a current of 10^{-15} A follows, which reaches the resolution limit of conventional amplifiers. To exceed the detection limit (of the Faraday cage), a secondary electron multiplier can be used. Therefore, an electron cascade is used to amplify the physical measurement signal by up to 10^3 depending on the species, which improves the detection limit to 10^{-14} mbar.[11]

The leakage rate of the system is made up of natural and artificial leakage rates. It is determined from the average change in pressure over time (Fig. 2) when the valve to the commercial pumping system is closed [Fig. 1(e)]. Before baking out, a leakage rate of 1.3×10^{-5} mbar l s^{-1} is measured. After baking out at 210 °C for 48 h, the leakage rate drops to 3.2×10^{-7} mbar l s^{-1}, and after that, subsequent heating of the getter-MEMS at 150 °C for 2 h further reduces it to 3.7×10^{-8} mbar l s^{-1}. With this heating, most of the physisorbed elements are removed from the system. That leakage rate is sufficiently low to be able to be compensated by the pump rate of the sputtered nonevaporable getters, which is to be expected to range between 0.437 and 3.94 mbar l s^{-1} cm^{-2} (H_2 and CO) depending on the gas type.[14] The difference between the leakage rates before and after the activation of all components in the amount of 1.3×10^{-5} mbar l s^{-1} describes the outgassing rate of the system and justifies the need for the bakeout process.

To generate a reproducible operating point for characterization, the four step process of initiation of the high vacuum test bench follows Malyshev *et al.*[15] In the first step, starting from atmospheric pressure, the system is pumped down to a high vacuum level of approximately 10^{-6} mbar with the pump system, which from now on always remains active. This is followed by the heating of the recipient, including the connection points to the measuring and pump system, at 210 °C for at least 48 h, while the getter-MEMS reaches a maximum of 80 °C. The recipient is then cooled to 150 °C. In this way, an improvement in the vacuum level of 10^{-7} mbar can be achieved. In the second step, the recipient and the getter-MEMS are heated further to a temperature of 150 °C [no pumping below 160 °C (Ref. 5)] for at least 2 h in order to remove the remaining physically bound molecules in the system while hindering the emitted molecules to adsorb at the recipient surfaces. This serves to increase the getter capacity for hydrogen and to improve the vacuum level. The recipient is cooled to room temperature and stays there for the remainder of the experiment. Therefore, the setup is ready for characterizing the getter-MEMS pumping functionality for UHV environments in the fourth step by means of a cold cathode gauge and a quadrupole mass spectrometer.

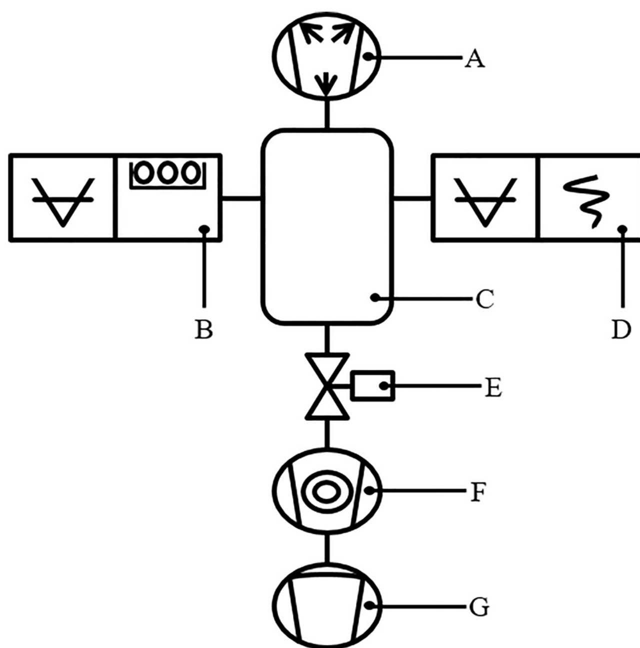

FIG. 1. Prepared, schematic drawing of the vacuum system (test rig) used in compliance with standardized symbols of DIN 28401 (Ref. 12), including getter-MEMS (a), cold cathode gauge (IKR271, b), vacuum chamber (c) quadrupol mass spectrometer (HAL301 RGA, d), pneumatic valve (e), and turbomolecularpump (HiPace 300H, f) with membrane backing pump (g).

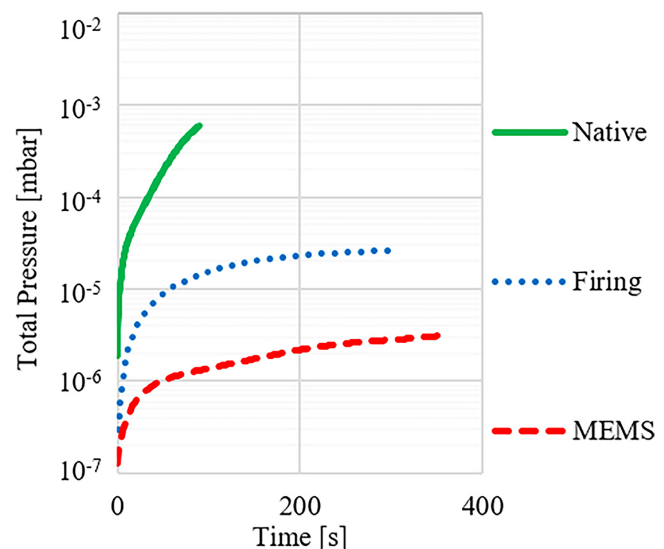

FIG. 2. Measurement of the total pressure over time to determine the leakage rates of the vacuum system with a closed valve [Fig. 1(e)] before "Native" and after "Firing" the recipient has been baked out, as well as after the getter-MEMS "MEMS" has been baked out.

Downloaded from http://pubs.aip.org/avs/jvb/article-pdf/doi/10.1116/6.0001991/16612541/054202_1_online.pdf

© Author(s) 2022

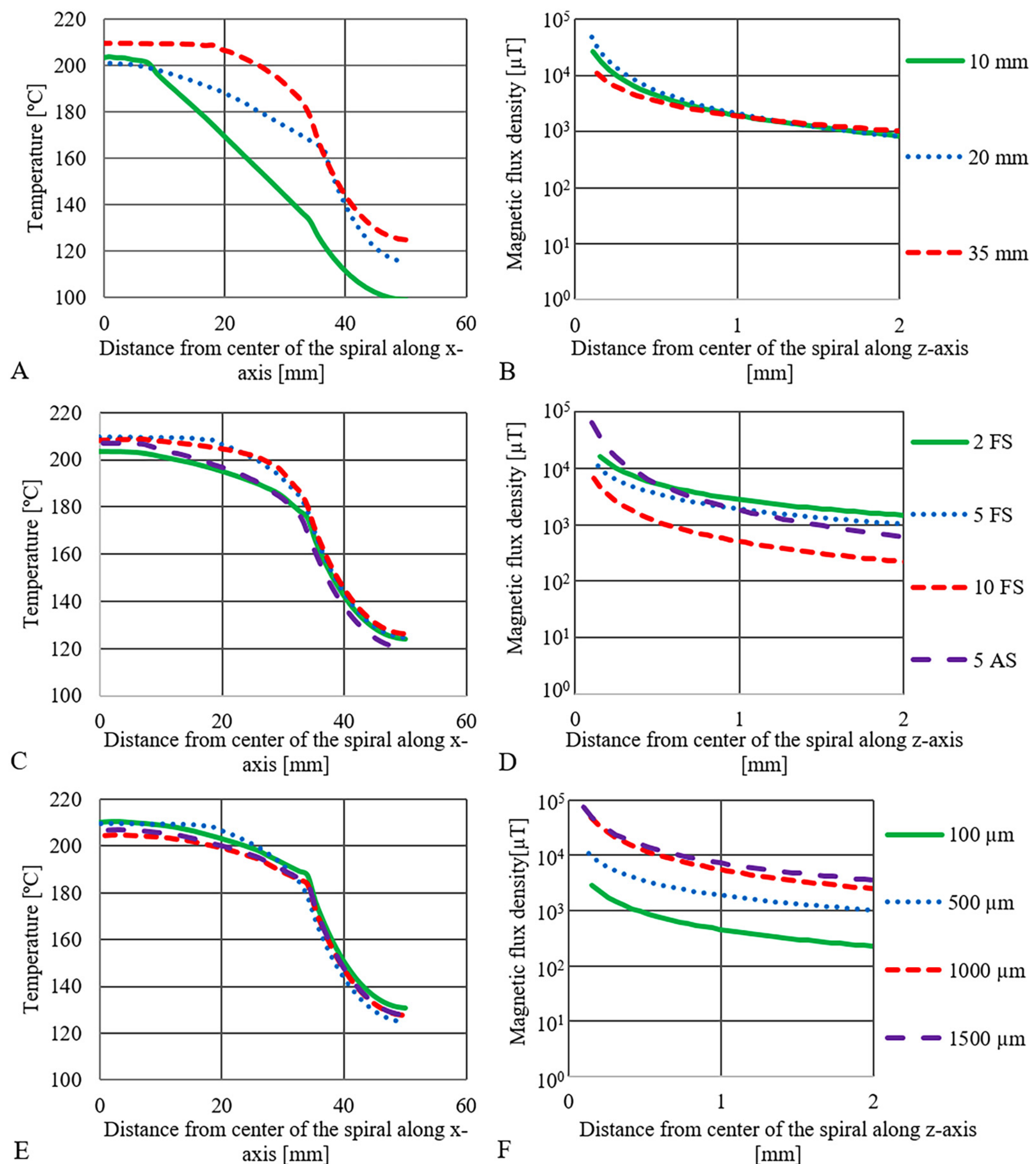

FIG. 3. Results of FEM simulations referring to a lateral temperature distribution along the *x* axis [(a), (c), and (e)] and vertical magnetic flux density [(b), (d), and (f)] for various parameters of spiral structure: Influence of the spiral diameter [(a) and (b)], of the spiral type (spiral S, Fermatian F, and Archimedean A), and the number of double turns [(c) and (d)—2–10 turns] and of a conductor track width [(e) and (f)].

III. MODELING

A. Theoretical conception

The getter-MEMS is a miniaturized resistance heater with an NEG coating on a glass substrate. Hierarchically, the design is initially carried out for the getter and, based on this, for the heating system and the associated components. The functions are used to derive the associated requirements, which are followed by the solutions for the individual system components.[16] With regard to the performance parameters of the surface and total bulk capacity of the getter coating, these are maximized through the selection and production of the material. The surface capacity is determined by the adsorption enthalpies, catalytic reactivity, porosity, and roughness. The total bulk capacity is characterized by the diffusion and solubility coefficients. In order to guarantee a specific functionality of the miniaturized NEG pump, a heating system must be used that keeps the getter exactly and evenly at the desired temperature over the entire surface in a minimum of time

Downloaded from http://pubs.aip.org/avs/jvb/article-pdf/doi/10.1116/6.0001991/16612541/054202_1_online.pdf

© Author(s) 2022

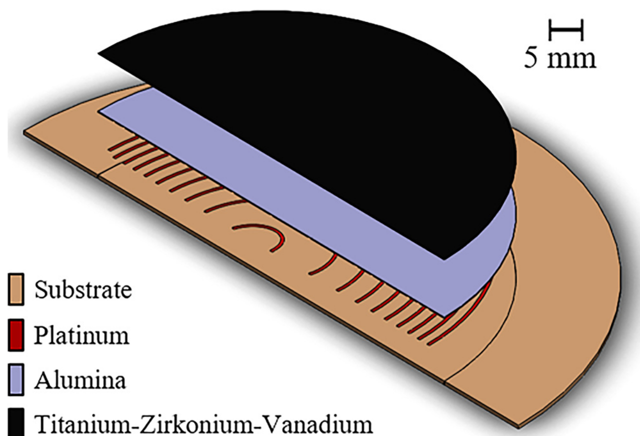

FIG. 4. Cross section (CAD design) of getter-MEMS in an exploded view of the simulated model with real dimensions. On top of the Borofloat substrate (bottom layer, 500 μm) is the platinum heater structure (400 nm) embedded in alumina (4000 nm) and on top of which is the getter coating (top layer, 3000 nm).

with adequate power and, therefore, minimizing any form of degradation. The generation of a preferred thermal direction starting from the resistor toward the getter plays a decisive influence. Therefore, the entirety of all components must be taken into account for the design of the system. The components of the system include the contacts, the insulation, the substrate, and the heating system. With regard to ideal temperature homogeneity, the geometry of the resistor structure is important, which is generally optimized by a bifilar structure.[17] The design optimization of the geometry is based on finite element simulations with ANSYS. All other performance parameters of the heating element are optimized with a platinum resistance layer, which is encased with titanium as an adhesion promoting layer. An insulating aluminum oxide layer and a Borofloat substrate are used for the getter coating (TiZrV) to maximize the preferred direction of heat and to minimize the coefficient of thermal expansion differences. In order to ultimately guarantee ideal contact with the UHV solder, the contact pads are reinforced with copper. In general, the chemical, mechanical, and thermal stability of the selected materials is also important. Furthermore, with regard to a potential application in a miniaturized magneto-optical trap, the materials must be electromagnetically neutral and be realizable using clean processing methods.[1] Overall, the connected dependencies between the components are multidimensional and influence each other destructively or constructively so that the degree of the respective characteristics must be weighed up.[17,18]

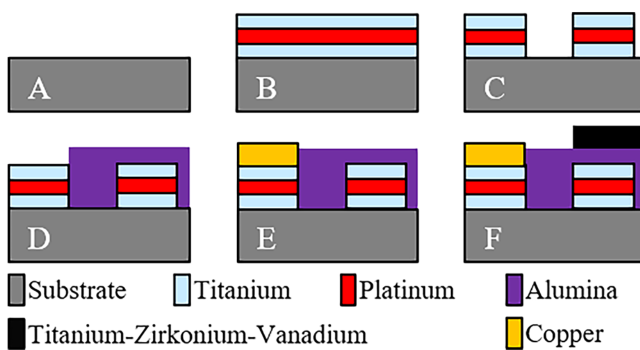

FIG. 5. Idealized, schematic production route of the getter-MEMS in a cross section in the border area between the electrode contact pad and the spiral edge area. The production takes place chronologically from (a) to (f). Starting from a blank substrate (a), various microsystem-technical processing steps (cf. text) take place, which enable the production of the getter-MEMS. Contact areas are exposed and reinforced with copper (e) for a subsequent soldering step, and the central spiral winding area is coated with the getter (f).

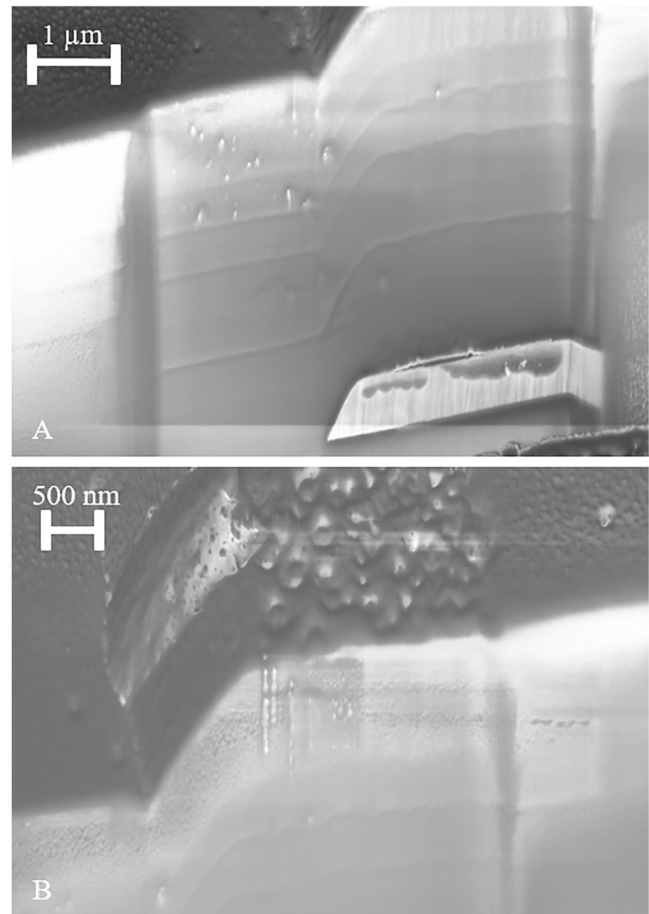

FIG. 6. SEM cross-sectional profile of the total getter-MEMS corresponding to Fig. 5(f) (a) and the SEM cross-sectional profile of the top surface (NEG and isolation) layers (b). The lower, lighter layer in A is characterized as the heating material (titanium-platinum-titanium), followed by several layers of aluminum oxide (alumina, gray dark). Boundary surfaces can be seen that result from the interim cleaning processes. Finally, as the uppermost, a slightly bright, already aged layer consisting of a titanium-zirconium-vanadium layer can be seen.

Downloaded from http://pubs.aip.org/avs/jvb/article-pdf/doi/10.1116/6.0001991/16612541/054202_1_online.pdf

© Author(s) 2022

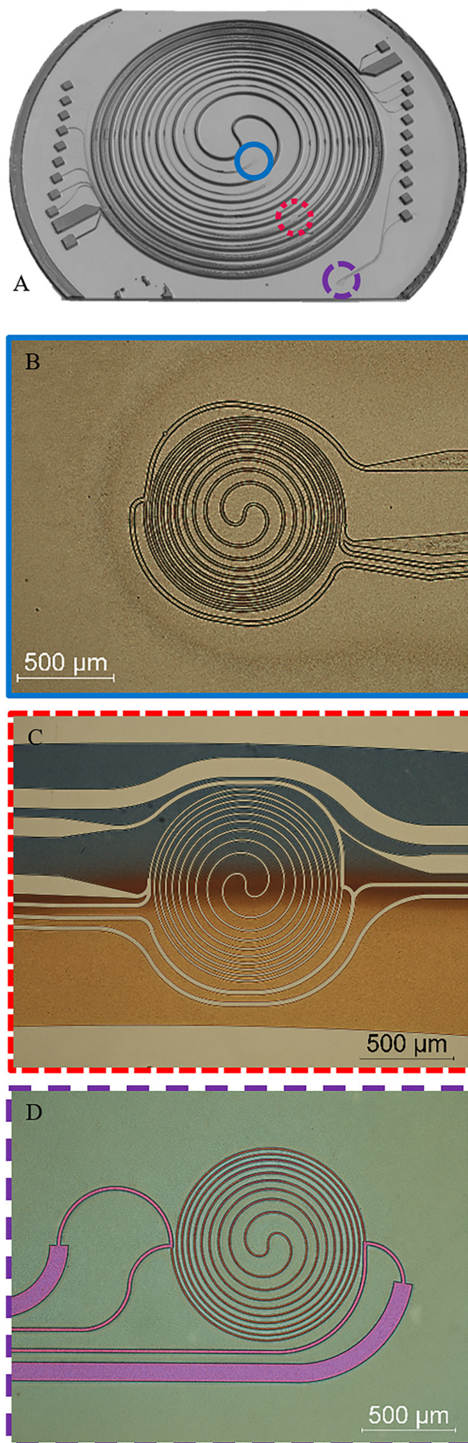

FIG. 7. Confocal micrograph of a structured microheater on a glass with markings for sensor 1 (blue line), sensor 3 (red small dashed line), and sensor 6 (purple big dashed line) (from the inside, a) and microscopic images of the getter-MEMS for sensor 1 (b), sensor 3 (c), and sensor 6 (d).

B. Numerical conception by FEM

Electrically thermally coupled numerical simulations were used to design the heating system with regard to the target parameter temperature distribution. The starting point is an adjusted heat flow density that results in 200 °C in the center of the spiral. Based on this, the necessary electrical supply of the system can be derived analytically, taking into account the electrical resistance. Within this framework, the diameter, the spiral type, the number of turns, the conductor track dimensions, and other parameters are varied. These parameters are systematically examined iteratively (i.e., only one parameter at a time). In the first iteration, the spiral radii from 10 to 35 mm are examined [Fig. 3(a)]. In the second iteration, the type of spiral is determined by comparing Archimedean (AS) and Fermatian (FS) spirals [Fig. 3(c)]. In the third iteration, the number of turns of 2–10 double turns (2–10 FS) is considered [Fig. 3(c)]. In the fourth iteration, the track width is varied between 100 and 1500 μm [Fig. 3(e)]. In summary, the parameterized simulations show that a slightly larger heater than the surface should be heated with Fermat's spiral structure with five double turns. The temperature profile can be further optimized by choosing a conductor track width of 500 μm and a geometric substrate structuring of the rear side (subtraction of the substrate in a ring and circular form) or by integrating a highly thermally conductive layer.[13]

In addition, the electromagnetic behavior of the coil along the Z dimension was simulated with respect to its application within a miniaturized magneto-optical trap. The example shows the magnetic flux density for the selected parameters during activation [Figs. 3(b), 3(d), and 3(f)]. All systems exceed the average, natural magnetic flux density of the earth's magnetic field for Europe (around 40 μT). It becomes clear that the selected structure minimizes the magnetic flux density within the height of the vacuum recipient (1 mm). This further investigation thus supports the results of the thermal simulations, which derive the structural design according to Fig. 4.

C. Production

A five-stage process chain for the production of the getter-MEMS was developed (Fig. 5). In addition to this idealized presentation, the MEMS is shown in a full SEM side profile [Fig. 6(a)] and focused on the NEG layer [Fig. 6(b)]. This includes the production and functionalization of the resistance structure of the microheater by means of cathode sputtering [Figs. 5(a)–5(c)]. Therefore, a platinum layer (400 nm) is encased by titanium adhesion layers (50 nm), which are further heated to its maximum operating temperature in order to be able to guarantee efficient operation later on and structured by means of photolithography and ion beam etching (1). Moreover, insulation between microheater and getter layers is guaranteed by depositing an aluminum oxide layer (4000 nm) by means of cathode sputtering. This requires extensive wet-chemical cleaning of the surface with an acidic piranha solution beforehand and a repetitive coating procedure, which needs to be interrupted by ultrasonic cleaning baths (2). Additionally, the contact areas outside of the spiral structure are exposed by means of photolithographic processing and reactive ion beam etching and filled

Downloaded from http://pubs.aip.org/avs/jvb/article-pdf/doi/10.1116/6.0001991/16612541/054202_1_online.pdf

© Author(s) 2022

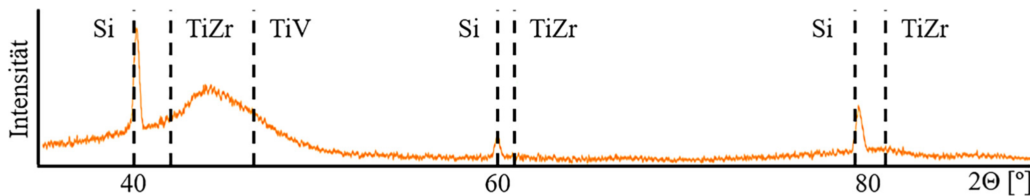

FIG. 8. XRD profile with relevant crystal orientations of the TiZrV layer, sputter deposited from a TiZrV composite target at 5×10^{-3} mbar with 550 W and 50 sccm argon (atmosphere) on a silicon wafer.

by depositing copper (800 nm) through cathode sputtering (3) [Figs. 5(d)–5(e)].

Figure 7(a) shows a fabricated microheater on a glass substrate, with marked individual temperature sensors. Last, the getter coating is produced within the contact areas, i.e., geometrically above the spiral windings using cathode sputtering [Fig. 5(f)]. To minimize the degree of contamination of the MEMS and, therefore, protect the sensitive getter capacity, the entire system is first baked out for at least 12 h at 200 °C in a high vacuum of 10^{-6} mbar in order to outgas all physically bound components. Shortly before the actual deposition, the vacuum in the system is freed from all getterable impurities by means of an *in situ* ion getter pump before a defined area (900 π mm^2) is coated with a 3150 nm getter at 550 W with an atmospheric pressure of 10^{-3} mbar with an argon carrier gas (4). Figures 7(b)–7(d) show the microscopic top view of sensor 1 below the getter layer, sensor 3 at the transition of the getter layer, and the isolated sensor 6.

Therefore. a nanocrystalline coating [compare broad 2-theta (Θ) peak at 43° in Fig. 8 by XRD and a crystallite size in Fig. 9(a). by SEM] consisting of a homogeneously distributed titanium, vanadium, and zirconium with a surface quality defined by $R_a = 4.27$ nm at $R_z = 43.5$ nm [compare surface profile in Fig. 9(b)

Downloaded from http://pubs.aip.org/avs/jvb/article-pdf/doi/10.1116/6.0001991/16612541/054202_1_online.pdf

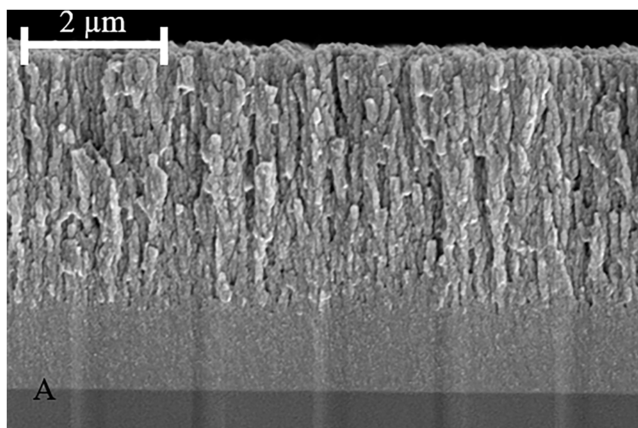

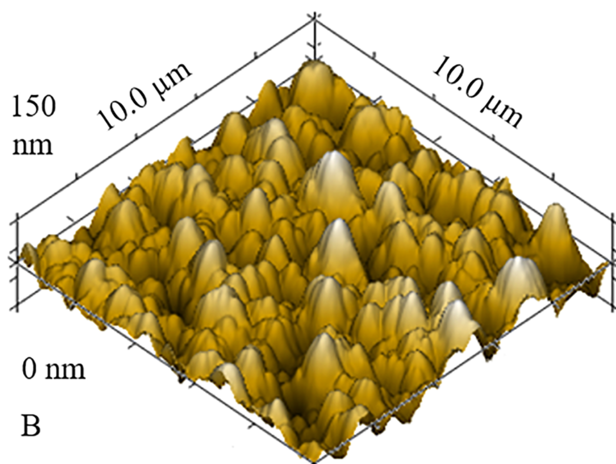

FIG. 9. SEM cross-sectional profile (a) and the AFM profile of the surface (b) of the TiZrV layer, sputter deposited from a TiZrV composite target at 5×10^{-3} mbar with 550 W and 50 sccm argon (atmosphere) on a silicon wafer.

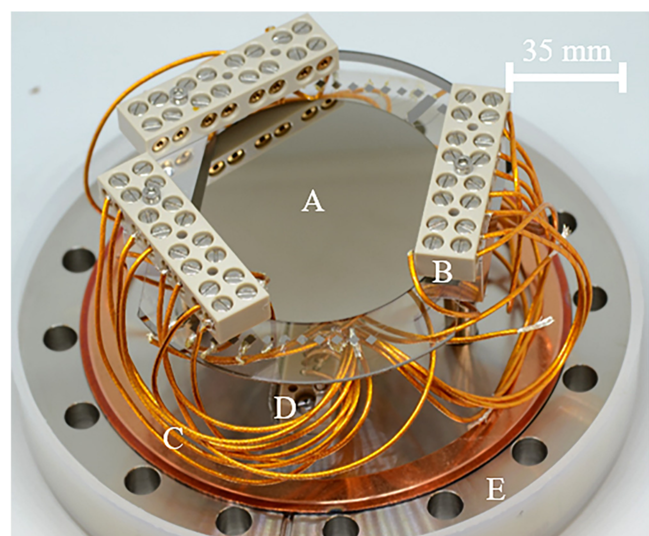

FIG. 10. Image of the getter-MEMS built into a CF-100 flange with a rewiring level, which is then built into the vacuum chamber (Fig. 1). The figure shows the isolated and contacted getter-MEMS (a), which is fixed using a bracket (b). This bracket also holds the electrical rewiring level and connects the MEMS via a UHV cable layer (c) to the electrical bushing (d) of the flange (e).

© Author(s) 2022

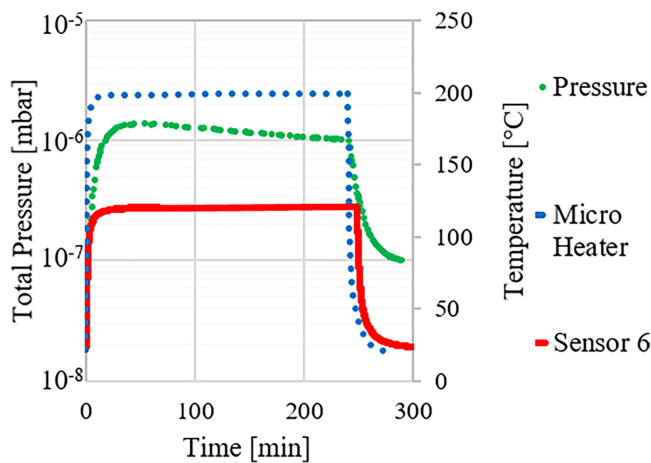

FIG. 11. Time course of the recipient total pressure and the temperature of the microheater and sensor 6 within a four-hour activation. The legend terms microheater and sensor 6 refer to the existing temperature and the pressure to the total pressure in the vacuum recipient.

by AFM] is created on the isolated microheater. Last, the electrical and mechanical contacting of the system takes place using 315-LF-Solder with 301-KAP-RIB15 cables for UHV applications. The microheater and the temperature sensor array temperature resistance dependencies are calibrated so that the getter-MEMS can be mechanically installed and be electrically connected to the rewiring level (Fig. 10).

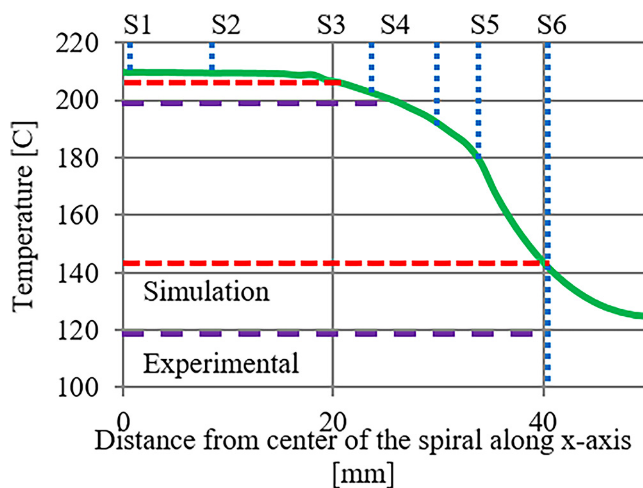

FIG. 12. Overview of the geometrical distribution of the temperature sensors [sensor 1 (S1) to sensor 6 (S6), blue small squares] on the system, showing the simulated (green line and red small line dotted) as well as experimental temperature curves (purple big line dotted, b).

IV. RESULTS AND DISCUSSION

A. Microheater

The microheater, including the temperature sensor array, is calibrated with respect to directive DIN 43764.[7] The system parameter temperature dependent electrical resistance properties are characterized in air before the system is deployed in vacuum.

Figure 11 shows the temperature behavior of the microheater (1400 Ω at 20 °C) and sensor 6 (1600 Ω at 20 °C, outside of the coil) during activation of the getter-MEMS over time and pressure in the recipient. To generate 200 °C at 1400 Ω resistance, the microheater requires 155 V in a high vacuum atmosphere. Therefore, the resistance changes from 1400 Ω to approximately 1950 Ω so that a final maximum current of 79.7 mA is induced, resulting in a total power consumption of 10 W [see Eq. (1)]. Based on this, the alpha coefficient of the sputtered layers can be calculated as $2.08 \times 10^{-3}\ \Omega\,°\text{C}^{-1}$ for the microheater and $1.61 \times 10^{-3}\ \Omega\,°\text{C}^{-1}$ for sensor 6, which differs from DIN IEC 751[19] with $3.88 \times 10^{-3}\ \Omega\,°\text{C}^{-1}$. The time until the maximum temperature is reached is calculated according to Eq. (2) to around 20 ms. However, experimentally, the system shows a significantly longer warm-up phase of around 240 s before reaching a maximum temperature. First, the start-up behavior of the voltage source limits the energy available and thus increases the warm-up time of the spiral. Second, conductive energy losses (i.e., cooling) through the surrounding mass must be considered.

Starting from the center of the spiral, Fig. 12 shows the simulated course of the temperature and the position of the integrated temperature sensors. In addition, the difference between the average temperature of the microheater and sensor 6 regarding numerical and experimental results is shown, which allows the gradient to be inferred. In general, the results confirm the predicted temperature gradient regarding the average temperature of the microheater structure and the external temperature sensor 6. The mean temperature gradient is calculated to approximately 80 °C and, therefore, has a deviation of 10 °C from the simulated results. The difference is as expected and can be explained by energy conduction from the microheater structures to the large area substrate. Furthermore, there is energy conduction to the large contact area of the system installed in the holder with the heat sink, i.e., the heat-conducting recipient. Basically, a certain temperature loss beyond the limits of the spiral is to be expected. This can be optimized in the long term by choosing less heat-conducting mounting structures. At the same time and the present pressure level of 1×10^{-7} mbar, heat conduction via the vacuum and heat radiation from the various surfaces are expected to be low but can be monitored and reduced in the long term.

In addition, guaranteeing temperature location resolution can be enabled through an optimized design. If the complexity of the heating structure remains the same, the following optimization potentials are available. This design is characterized, first, by conductor webs of the current and potential contacts of the temperature sensors that are more than 100 μm apart and have more than 100 μm width when process-related contaminations cannot be excluded. Second, the design can be optimized by increasing the contact pad area from 2×2 to at least $4 \times 4\ \text{mm}^2$. Therefore, a layer structure of a titanium adhesion promoter (50 nm) on a roughened heater layer (by sputter

Downloaded from http://pubs.aip.org/avs/jvb/article-pdf/doi/10.1116/6.0001991/16612541/054202_1_online.pdf

© Author(s) 2022

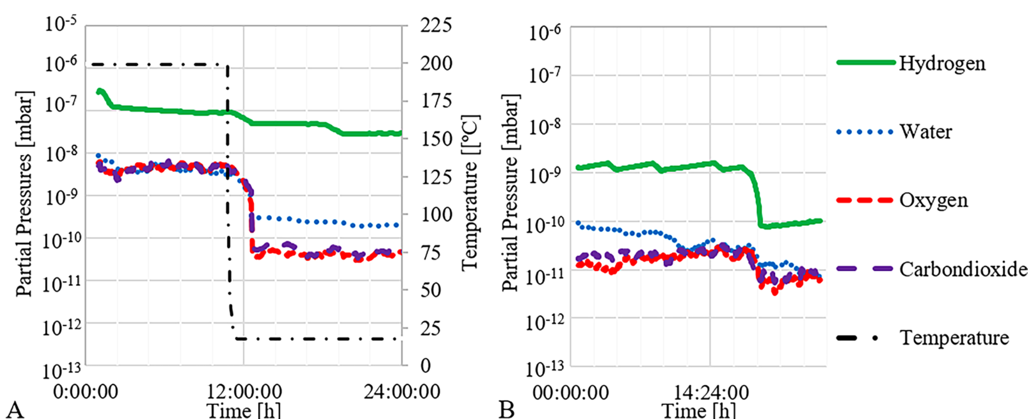

FIG. 13. Residual gas analysis (a) by means of a mass spectrometer for hydrogen, water, oxygen, and carbon dioxide averaged over time at and after the preactivation (6 h at 200 °C, measured with a Faraday detector) as well as over time at and after activation (10 h at 200 °C, measured with a secondary electron multiplier detector, b). At the beginning of the measurement, the getter is at the activation temperature.

Downloaded from http://pubs.aip.org/avs/jvb/article-pdf/doi/10.1116/6.0001991/16612541/054202_1_online.pdf

etching) followed by 500 nm copper and 20 nm gold including a diffusion protection layer can be recommended.

B. Getter-MEMS

It is known from the literature that the temperature must exceed a defined activation temperature in order to activate the surface as well as fall below that temperature to enable pumping.[3,20] This activation temperature is specific for the pumping getter component as well as the compounds to be pumped (see the differential pressure change over time, Fig. 13) and is also influenced by the lateral (heat-) distribution of these getter atoms on the surface.[20] These and other effects control the general shape of the s-shaped curve and the gradient at the apex of the course of the partial pressures (Fig. 13).

Referring to the total pressure curve of the initialization process, a pressure level of 10^{-9} mbar can be reached by preactivation at 200 °C for 6 h. This pressure level can be improved by full activation at 200 °C for 12 h to at least 10^{-10} mbar, reaching the detector measurement limit of 10^{-10} mbar. At the same time, partial pressures of the reactive gases, that is, of carbon mono- and dioxide, oxygen as well as nitrogen mono- and dioxide and water, can be decreased to a pressure level of 10^{-9}–10^{-10} mbar in the preactivation and to a pressure level of up to 10^{-11}–10^{-13} mbar in full activation. In a first estimate, e.g., for water, suction power calculates [Eq. (4)] to 3.0×10^{-12} mbar l s^{-1}, and therefore, a pumping power [Eq. (3)] of 2.9×10^{-3} l s^{-1} or 1.9×10^{-5} l s^{-1} cm^{-2} follows, resulting in a partial pressure for water of 1×10^{-9} mbar after full activation. The experimentally determined values are shown in Table I and differ as seen in Fig. 13. Due to its physical nature, the hydrogen pumping capacity is limited, making it the residual component in UHV applications. All other reactive components can be pumped more or less well, i.e., be removed from the residual gas.

The calculation of the suction and pumping capabilities is subject to a level of uncertainty, which results from the hardware-technical setup of the experiment and its framework conditions. The uncertainty in relation to the experiment setup takes into account the partial reduction of the partial pressures of the respective elements within the pumping processes up to the measurement limits of the respective detectors, which is 10^{-10} mbar for the Faraday [Fig. 13(a)] and 10^{-3} mbar for the SEM detector [Fig. 13(b)].[11] The uncertainty in relation to the framework conditions of the experiment in the parameter characterization is concerned with the unknown flow conductance and the element-dependent (especially for hydrogen), mathematically not considered effective leakage. This effective leakage equates the leakage rates of the chamber components of 10^{-8} mbar l s^{-1} and of the quadrupole mass spectrometer of 10^{-8} mbar l s^{-1} (during active operation) with the pressure-dependent suction power of the cold cathode

TABLE I. Experimentally determined suction and pumping power of the getter-MEMS for different residual gases at 10^{-8} mbar total pressure in a recipient (Fig. 1) with a total volume of 2 l. The suction powers (and pumping powers) are calculated from the steepest gradient in the change in the partial pressure over time [compare Eqs. (3) and (4) and Fig. 13].

Parameter	Unit	Hydrogen	Water	Nitrogen	Oxygen	Carbon dioxide
Suction power	mbar l s^{-1}	4.9×10^{-11}	3.0×10^{-12}	2.8×10^{-12}	1.7×10^{-12}	2.2×10^{-12}
Pumping power	l s^{-1}	4.9×10^{-2}	2.9×10^{-3}	2.8×10^{-3}	1.7×10^{-3}	2.2×10^{-3}
Pumping power	l s^{-1} cm^{-2}	3.2×10^{-4}	1.9×10^{-5}	1.8×10^{-5}	1.1×10^{-5}	1.4×10^{-5}

© Author(s) 2022

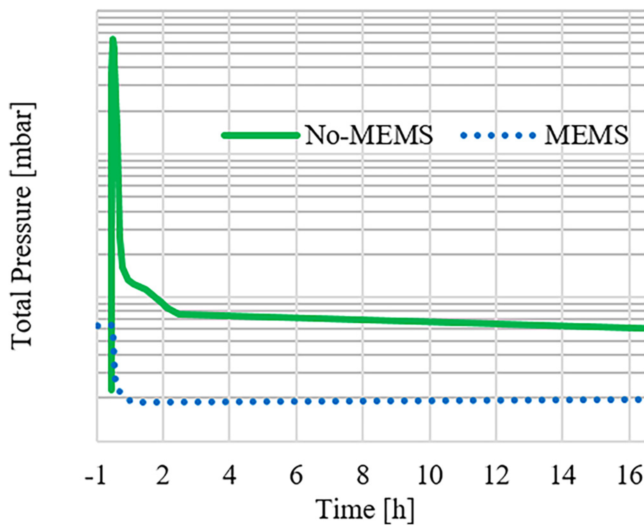

FIG. 14. Total pressure curve of the high vacuum chamber with a closed vacuum valve to the turbomolecular pump in two configurations to validate usability of getter-MEMS ability to maintain vacuum. Configuration 1 "No-MEMS" has no build in getter-MEMS and has only the pressure gauge IKR 270 active. Configuration 2 "MEMS" has a build in getter-MEMS that has been activated for 6 h at 200 °C with a partially activated pressure gauge IKR 270.

vacuum meter and the turbomolecular pump. A comparison with industrial, macroscopic getter systems was not meaningful since the performance parameters are determined by different characterization procedures as well as for other pressure regimes (10^{-6} mbar) and, therefore, under different physical conditions.

To confirm the application capability of the high vacuum pump for usage in a miniaturized MOT, the MEMS is investigated in the high vacuum test rig in two configurations (Fig. 14). In configuration 1 (No-MEMS), only the pressure gauge is installed and continuously active. In configuration 2 (MEMS), the getter-MEMS is also installed and baked out for 6 h at 200 °C at the start time. The pressure is partially measured by temporarily switching on the pressure gauge until the measurement signal has stabilized. At a pressure level of 10^{-7} mbar, we obtain an average total suction power of 3.5×10^{-10} mbar l s^{-1} and an effective total suction power of 2.8×10^{-10} mbar l s^{-1} (including suction power of the pressure gauge) of the getter-MEMS results. Therefore, the pressure initially increases to 8×10^{-7} mbar during its activation, reduces to a minimum of 3.5×10^{-7} mbar at the end of the activation (at 0 h), and reduces to a minimum of 1.5×10^{-7} mbar during cooling, following an increase to a final pressure of the system around 2.5×10^{-7} mbar. Comparing the course of the total pressure of the two configurations, a strong mitigation of the pressure pulse emitted (at the beginning of the experiment) when closing the shutter can be observed with the getter-MEMS configuration.

TABLE II. Theoretical consideration of the system parameters to assess the getter functionality for use in a miniaturized MOT based on experimental data of this work, compared to theoretical data (specifications) reproduced from Ref. 1.

	Unit	Micro-MOT (Ref. 1)	Getter-MEMS
Recipient volume	mm^3	7.5×10^2	2.0×10^6
Recipient surface	mm^2	7.9×10^2	2.6×10^5
Active NEG surface	mm^2	3.3×10^2	2.9×10^3
Surface ratio NEG to chamber		2.4×10^0	8.8×10^1
Particle density at 10^{-7} mbar in recipient volume		1.9×10^9	5.3×10^{12}
Particle per active NEG surface	mm^{-2}	6.0×10^6	1.8×10^9
Effective particle per active NEG surface	mm^{-2}	2.5×10^6	2.1×10^7

The volume in cubic millimeters of the recipient is calculated for a two-part cylinder consisting of one component with a height of 300 mm and a diameter of 100 mm and one component with a height of 20 mm and a diameter of 60 mm so that in total, 2.6×10^5 mm^3 follows (Table II). First, this results in a ratio of a getter surface to a recipient surface of 1:88 (corresponding 1:2.4 at Micro-MOT), which represents the probability that a particle will interact with the getter surface. Second, at a pressure level of 10^{-7} mbar, the volume will hold 10^{12} atoms (ideal gas approximation). These atoms are distributed over the getter surface, resulting in a ratio of 1.8×10^9 atoms per active surface area (mm^2). In comparison with the Micro-MOT according to Rushton *et al.*,[1] a ratio of 6×10^6 atoms per active surface area (mm^2) arises. Here, the smaller volume of the MOT (7.5×10^2 mm^3) contains correspondingly fewer particles (10^9 atoms) but has a larger active surface area in proportion. The interaction probability, calculated from the area ratios of the chamber and the active NEG surface, must be taken into account. This means that the active area of the getter-MEMS would have to be increased by a factor of 8.3 in order to achieve a comparable particle density per square millimeter considering the total recipient volume. With regard to Nordmann,[14] sputtered thin layers of TiZrV have a surface capacity for a carbon monoxide of 1.56×10^{13} atoms per square millimeter. Given these values, saturation has to be expected, but this saturation of the layers is volume-dependent and, at these pressure levels, time-dependent. The volume dependency can be taken into account using another factor and reduces the active surface of the NEG in the getter-MEMS. In summary, it can be deduced that the expected pump rates will be comparable, which ultimately only needs to be confirmed experimentally.

V. SUMMARY AND CONCLUSIONS

We report the development of a miniaturized high vacuum pump in the form of a getter-MEMS. For this purpose, the microsystem is determined step-by-step based on a qualitative discussion following the state of the art, combined into a rough concept and designed in detail by numerical simulations. In order to optimize pumping properties, homogeneous temperature application is

Downloaded from http://pubs.aip.org/avs/jvb/article-pdf/doi/10.1116/6.0001991/16612541/054202_1_online.pdf

© Author(s) 2022

essential. Therefore, the simulations focus on the homogenization of the temperature profile of the getter coating for which the diameter, the spiral type, the number of turns, the conductor track dimensions, and other parameters of the microheater are examined. In general, we can confirm the superiority of the spiral structure of a heating element in terms of homogenizing the temperature in the target area (comparing to Spruit *et al.*[17] and Baroncini *et al*[18]). In addition, we find that the homogeneity of the temperature profile is optimized by further parameters, including size, number of turns, and conductor track width.

A production process is developed and carried out for the target system so that the microsystem can be reproducibly characterized in a high vacuum test bench. First, there is a significant reduction in the overall pressure profile (i.e., pumping) to less than 10^{-10} mbar with the support of active pump technology (turbomolecular pump), broken down using the partial pressure curve for relevant residual gases. Second, the getter-MEMS enables the necessary pressure level to be maintained for use in an MOT of less than or equal to 10^{-7} mbar for more than 22 h without the support of active pump technology. Both characterizations were based on a 10 h activation of the getter layer at an average temperature of 220 °C, which was generated by approximately 10 W. A quantitative analysis of the pump properties is pending and can be carried out, for example, by a transmission measurement according to Nordmann,[14] which also enables a correlation of the sticking coefficient factor with the help of a ventilation (leak) system. Further, with regard to the present characterization, the correlation between pumping power and required energy is not expedient.

Regarding the initial characteristics of the pump, it will be necessary to establish a connection between the production-specific properties (i.e., arithmetic mean roughness, roughness depth, crystal structure, crystallite size, specific electrical resistance) of the coating and the resulting pump properties (pumping power, surface capacity, bulk capacity), monitored using suitable sensor technology. This technology should be able to control the getter temperature and capacity saturation and could be realized by half-bridge sensor technology. Moreover, promising approaches for the catalytic functionalization of this layer to decompose hydrogen and, thus, increase pumping capabilities should be evaluated.[21] Subsequently, the miniaturization and integration of the microsystem into the MOT has to follow.

ACKNOWLEDGMENTS

This work was funded by the Deutsche Forschung sgemeinschaft (DFG, German Research Foundation) under Germany's Excellence Strategy—EXC-2123 QuantumFrontiers—390837967. Furthermore, we would like to thank Hiden Analytical and Pfeiffer Vacuum for disclosing the functionality and calibration of the measurement peripherals used.

AUTHOR DECLARATIONS

Conflict of Interest

The authors have no conflicts to disclose.

Author Contributions

Leonard Frank Diekmann: Conceptualization (lead); Data curation (lead); Formal analysis (lead); Investigation (lead); Methodology (lead); Software (lead); Supervision (equal); Validation (equal); Visualization (lead); Writing – original draft (lead); Writing – review & editing (lead). **Alexander Kassner:** Conceptualization (supporting); Data curation (supporting); Formal analysis (supporting); Funding acquisition (equal); Investigation (supporting); Methodology (supporting); Project administration (equal); Resources (equal); Software (supporting); Supervision (equal); Validation (equal); Visualization (supporting); Writing – original draft (supporting); Writing – review & editing (supporting). **Folke Dencker:** Conceptualization (supporting); Data curation (supporting); Formal analysis (supporting); Funding acquisition (equal); Investigation (supporting); Methodology (supporting); Project administration (equal); Resources (equal); Software (supporting); Supervision (equal); Validation (equal); Visualization (supporting); Writing – original draft (supporting); Writing – review & editing (supporting). **Marc Christopher Wurz:** Conceptualization (supporting); Funding acquisition (equal); Investigation (supporting); Methodology (supporting); Project administration (equal); Resources (equal); Supervision (equal); Validation (equal); Visualization (supporting); Writing – original draft (supporting); Writing – review & editing (supporting).

DATA AVAILABILITY

The data that support the findings of this study are available from the corresponding author upon reasonable request.

REFERENCES

[1] J. A. Rushton, M. Aldous, and M. D. Himsworth, Rev. Sci. Instrum. **85**, 121501 (2014).

[2] E. Maccallini, F. Siviero, A. Bonucci, A. Conte, P. Srivastava, and M. Paolo, AIP Conf. Proc. **1451**, 24 (2012).

[3] C. Benvenuti, J. M. Cazeneuve, P. Chiggiato, F. Cicoira, A. Escudeiro Santana, V. Johanke, V. Ruzinov, and J. Fraxedas, Vacuum **53**, 219 (1999).

[4] C. Benvenuti, CERN Rep. **1211**, 200 (1998), available at https://accelconf.web.cern.ch/e98/papers/thz02a.pdf.

[5] C. Benvenuti, P. Chiggiato, A. Mongelluzzo, A. Prodromides, V. Ruzinov, C. Scheuerlein, M. Taborelli, and F. Levy, J. Vac. Sci. Technol., A **19**, 2925 (2001).

[6] A. E. Prodromides, C. Scheuerlein, and M. Taborelli, Vacuum **60**, 35 (2001).

[7] German Institute for Standardization (DIN), "Measuring, controlling, regulating: Electrical temperature sensors," DIN 43764 (1986).

[8] K. Jouston, *Handbuch Vakuumtechnik* (Springer Vieweg, Wiesbaden, 2018).

[9] German Institute for Standardization (DIN), "Vacuum technology—Standard procedure for measuring the performance data of vacuum pumps," DIN ISO 21360 (2012).

[10] D. Salzer, "IKR 270 Cold Cathode Gauge—Operating Instructions," Pfeiffer Vacuum, 28 February2022; see: https://www.pfeiffer-vacuum.com/filepool/file/measurement/bg5008ben_a.pdf?referer=1830&detailPdoId=3866&request_locale=en_US.

[11] P. Hatton and D. Lundie, "Mass Spectrometry in Real Time," Hiden Analytical Ltd., Labmate UK & Ireland, July 2020; see: https://content.yudu.com/web/14zjy/0A1wpyz/LMUK45.5/html/index.html?page=8.

[12] German Institute for Standardization (DIN), "Vacuum technology—Graphical symbols—Summary," DIN 28401 (2008).

Downloaded from http://pubs.aip.org/avs/jvb/article-pdf/doi/10.1116/6.0001991/16612541/054202_1_online.pdf

© Author(s) 2022

[13]German Institute for Standardization (DIN), “Vacuum gauges—Calibration by direct comparison with a reference gauge,” DIN ISO 3567 (2015).
[14]D. Nordmann, “Application of the transmission method for *in situ* characterization of a Ti-Zr-V NEG layer,” dissertation (Technical University of Central Hesse, 2014).
[15]O. B. Malyshev, K. J. Middleman, J. S. Colligon, and R. Valizadeh, J. Vac. Sci. Technol., A **27**, 321 (2009).
[16]Association of German Engineers (VDI), “Design of technical products and systems. Configuration of individual product design processes,” VDI 2221 (2019).
[17]R. G. Spruit, J. T. van Omme, M. K. Ghatkesar, and H. H. P. Garza, J. Microelectromech. Syst. **26**, 1165 (2017).
[18]M. Baroncini, P. Placidi, G. C. Cardinali, and A. Scorzoni, Sens. Actuators, A **115**, 8 (2004).
[19]German Institute for Standardization (DIN), “Industrial platinum resistance thermometers and platinum temperature sensors,” DIN EN IEC 60751 (2019).
[20]K. Masek, F. Sutara, T. Skala, J. Drbohlav, K. Veltruska, and V. Matolin, J. Vac. Sci. Technol., A **21**, 797 (2003).
[21]T. Miyazawa, Y. Kano, Y. Nakayama, K. Ozawa, T. Iga, M. Yamanaka, A. Hashimoto, T. Kikichui, and K. Mase, J. Vac. Sci. Technol., A **37**, 021601 (2019).

Downloaded from http://pubs.aip.org/avs/jvb/article-pdf/doi/10.1116/6.0001991/16612541/054202_1_online.pdf

© Author(s) 2022